Electronic Supplementary Information (E.S.I.).

High efficiency Cu_2ZnSnS_4 solar cells over FTO substrate and its CZTS/CdS interface passivation via thermal evaporated Al_2O_3.

Esteban Ojeda-Durán,*[a] Karim Monfil-Leyva,[a] Jacob Andrade-Arvizu,[b] Ignacio Becerril-Romero,[b] Yudania Sánchez,[b] Robert Fonoll-Rubio,[b] Maxim Guc,[b] Zacharie Jehl Li-Kao,[c] José A. Luna-López,[a] Edgardo Saucedo.[c]

Complete detailed process of metallic deposition and sulfurization process. The metallic films deposited by DC magnetron sputtering were deposited with the following characteristics: **Sample A:** Cu (193 nm)/ Sn (300 nm)/ Zn (180 nm); **Sample B:** Cu (190 nm)/ Sn (260 nm)/ Zn (170 nm), and **Sample C:** Cu (210 nm)/ Sn (290 nm)/ Zn (205 nm). After deposition, the CZT precursors were simultaneously sulfurized inside of a graphite box containing sulfur (100 mg) and tin (50 mg) powders, using a tubular furnace and the following two-step annealing: 15 min at 250°C (1 mbar Ar flux) and 30 min at 570°C (1 bar total Ar pressure) as is shown in Fig. S1.

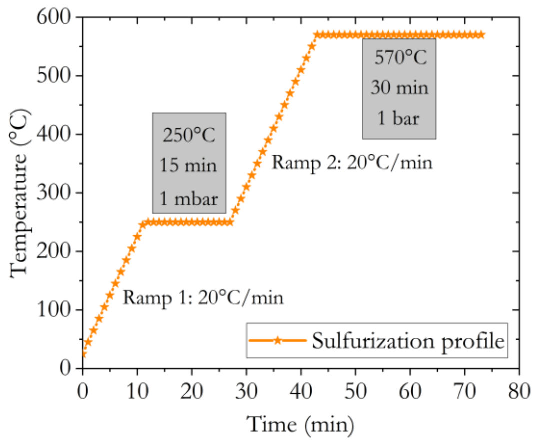

Fig. 1. Sulfurization profile for obtaining CZTS films.

The cationic ratios after sulfurization are shown in Table SI.

Table SI. Cationic ratios of CZTS films.

Sample	Zn/Sn	Cu/(Zn+Sn)
A	1.0	0.7
B	1.1	0.76
C	1.2	0.73

With the aim to passivate the CZTS/CdS due to a possible surface defects we deposited an Al_2O_3 layer onto CZTS and then CdS was deposited by chemical bath deposition. CdS, i-ZnO, and ITO were deposited in the same batch in both structures FTO/Mo (20 nm)/CZTS and FTO/Mo (20 nm)/CZTS/Al_2O_3 to avoid some differences in composition. In Fig. S2 are shown the solar cell structures of samples without Al_2O_3 (Fig. S2a) and samples with Al_2O_3 (Fig. S2b).

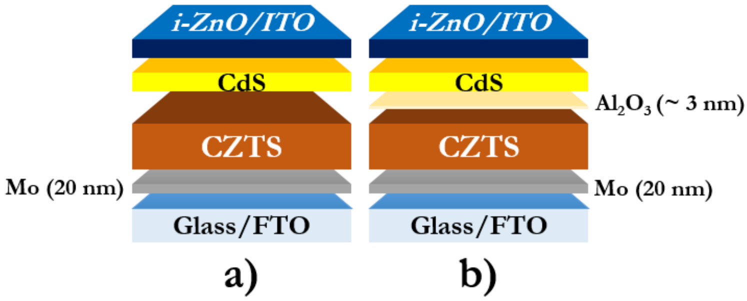

Fig. S2. Solar cell structures on FTO substrate a) FTO/Mo(20 nm)/CZTS/CdS/i-ZnO/ITO and b)FTO/Mo(20 nm)/CZTS/Al_2O_3/CdS/i-ZnO/ITO.

Compositional, morphological, and structural analysis from the as-grown CZTS films. Before the final device fabrication (CdS deposition and so on), samples A (Cu/(Zn+Sn)=0.7 & Zn/Sn=1.0), B (Cu/(Zn+Sn)=0.76 & Zn/Sn=1.1), and C (Cu/(Zn+Sn)=0.73 & Zn/Sn=1.2), were analyzed by Raman (λ=532 nm) to confirm the good crystalline quality. In Fig. S3 are shown the Raman spectra from samples A, B, and C. All the samples showed the characteristic peaks related to CZTS [S1]. Moreover, FWHM from the Raman spectra was calculated. The FWHM values were 6.48 cm^{-1} (sample A), 6.34 cm^{-1} (sample B), and 6.11 cm^{-1} (sample C) in FTO substrate. FWHM values were obtained in the range 5-8 cm^{-1}, which confirms the good crystalline quality [S1]. On the other hand, in the inset fig in Fig. S3 is shown the Raman spectra under 325 nm of excitation. The three samples showed traces of ZnS and, as consequence, this can affect in optoelectronic properties in solar cells.

In Fig. S4 a), b), and c) are shown the top-view images from the as-grown films A, B, and C, respectively. The images were taken from CZTS onto SLG substrate. In Sample A, grains showed many voids between them, these voids were related to the production of volatiles (tin compounds). In comparison with Samples B and C, there were a trend related with Zn/Sn ratios: supposing that with a major quantity of tin (major production of volatiles) there are major quantity of voids. In principle, the surface voids could severely affect the properties of the solar cells by decreasing the shunt resistance and deteriorating the FF. In the same way, Sample B found a perfect equilibrium in quantity of Cu, Zn, and Sn, that could help to a perfect balance in Cu_{Zn} and V_{Cu} defects, comparing with Samples A and C, and, as consequence, showing better efficiencies in sample B. All the samples showed large amounts of small crystallites at the surface that are associated to the presence of ZnS secondary phase [S2,S3].

These small crystallites seem to be reduced for lower Zn contents as expected. Finally, the average grain sizes were 1.5 µm, 1.3 µm, and 1.6 µm, respectively.

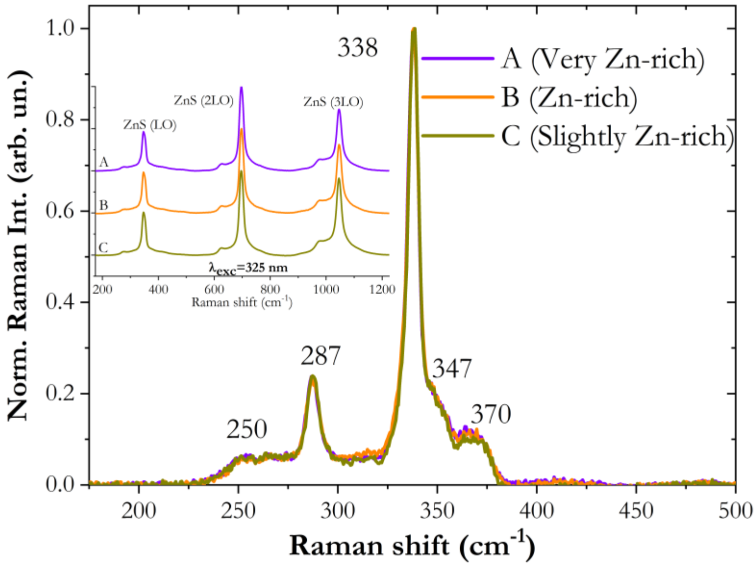

Fig. S3. Raman spectra from as-grown samples A, B, and C, on FTO substrate excited with 532 nm of wavelength. Inset figure. Raman spectra from as-grown samples A, B, and C on FTO substrate excited with 325 nm of wavelength.

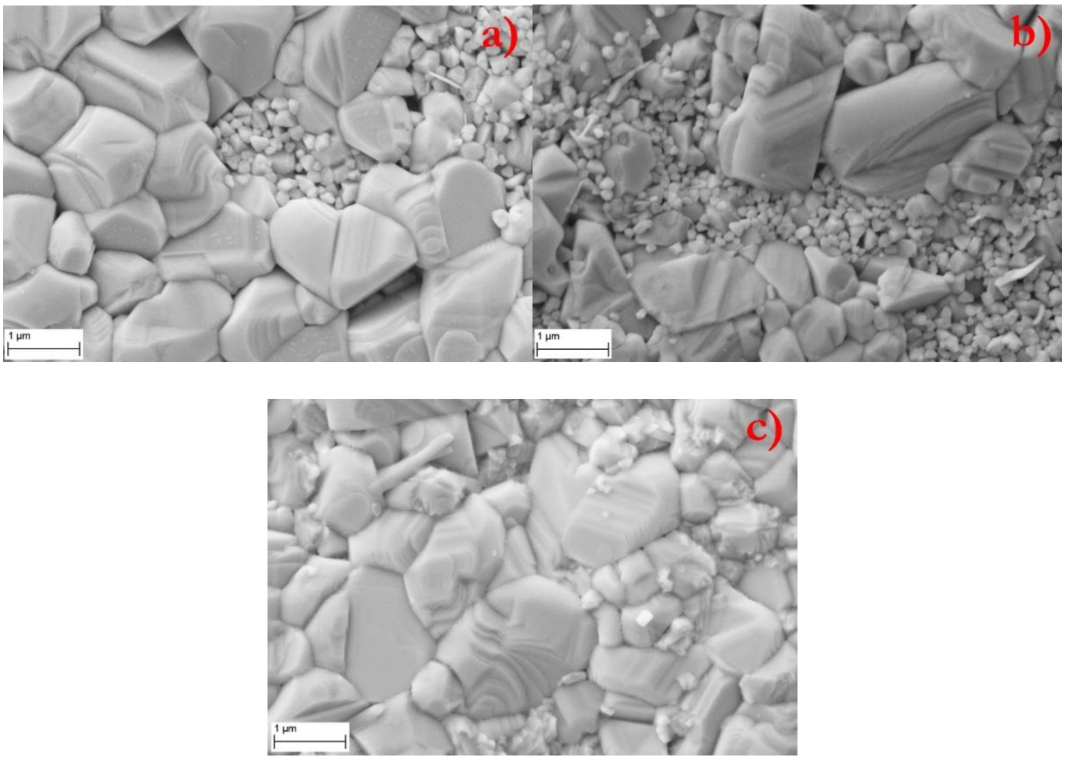

Fig. S4. Top-view SEM images from the as-grown films. (a) A, (b) B, and (c) C.

Optoelectrical analysis from all CZTS solar cells. In Fig. S5 (Supporting Information) are shown the box-plot diagrams from the samples BNA & BWA. The box-plot diagrams from complete samples: BNA and BWA (10 solar cells in each sample) were analyzed. BWA sample showed clear increases in V_{oc} and J_{sc} box-plot diagrams reaching 704 mV and 18.3 mA/cm^2 as maximum values. The increase in V_{oc} can be attributed to the Al_2O_3 interlayer on the CZTS solar cell [S4, S5, S6]. In contrast, FF and efficiency box-plot decreased. BNA showed FF of 65% and an efficiency of 7.7%. On the other hand, BWA showed FF of 57.7% and an efficiency of 7.3% as maximum values. In the same regard, the box-plot of BWA sample showed better uniformity in efficiency due to Al_2O_3 passivation.

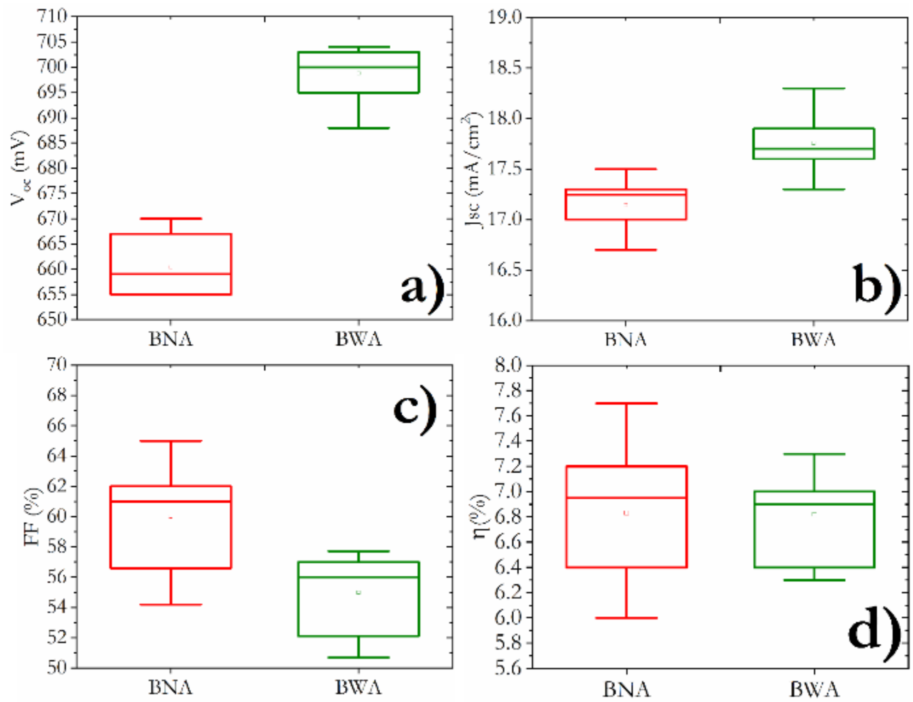

Fig. S5. Box-plot diagram of the samples BNA & BWA showing a) V_{oc}, b) J_{sc}, c) FF, and η. Ten CZTS solar cells were fabricated per each sample (10 solar cells on BNA sample and, 10 solar cells on BWA sample).

In Fig. S6. (Supporting Information) are shown the J-V curves from CZTS solar cells without Al_2O_3 (Fig. S6a) and with Al_2O_3 (Fig. S6b). In Fig. S6a) sample ANA showed an efficiency of η = 4.9% and sample AWA (Fig. S6b) showed an η = 5.5%. The difference between them in V_{oc} was 39 mV which is an important improvement. The Fill Factor in both solar cells are quite similar. The sample CNA showed an η=4.9% (Fig. S6a) and sample CWA showed an η=4.4% (Fig. S6b). The difference of the increment of V_{oc} is 17 mV with the use of Al_2O_3. The FF decreased from 56.4% to 50.7%.

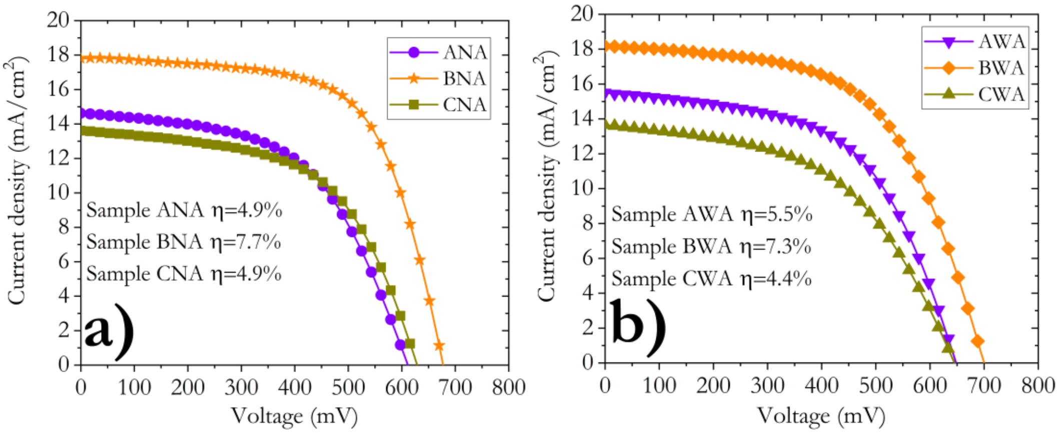

Fig. S6. J-V curves from solar cell devices a) ANA, BNA, and CNA and b) AWA, BWA, and CWA.

The J-V dark curves were using to obtain G_{sh}, R_s, A and J_0. To obtain G_{sh} it must be plotting the dJ/dV vs V. Shunt resistance (R_{sh}) values were calculated with the inverse of shunt conductance values. To obtain the R_s and the ideality factor (A), it must be plotting the dV/dJ vs $(J+Jsc)^{-1}$, and finally you can plot [ln(J-G_{sh}V)] vs [V-R_sJ] to obtain the J_0 [S7]. In Fig. S7 are shown the curves to obtain G_{sh} values from samples without Al_2O_3 (a) and with Al_2O_3 (b). The solar cell with the best shunt resistance is sample BNA. In the same way, BWA showed lower shunt resistance than BNA, despite of Al_2O_3 interlayer. In the same regard, samples AWA & CWA showed R_{sh} values of 4,347.9 Ω/cm^2 and 1,639.4 Ω/cm^2, both samples showing an improvement in shunt resistance due Al_2O_3 interlayer. With the passivation by Al_2O_3, the shunt paths effect decreased in samples A and C; these shunt paths could help to some carriers can travel through the device [S8].

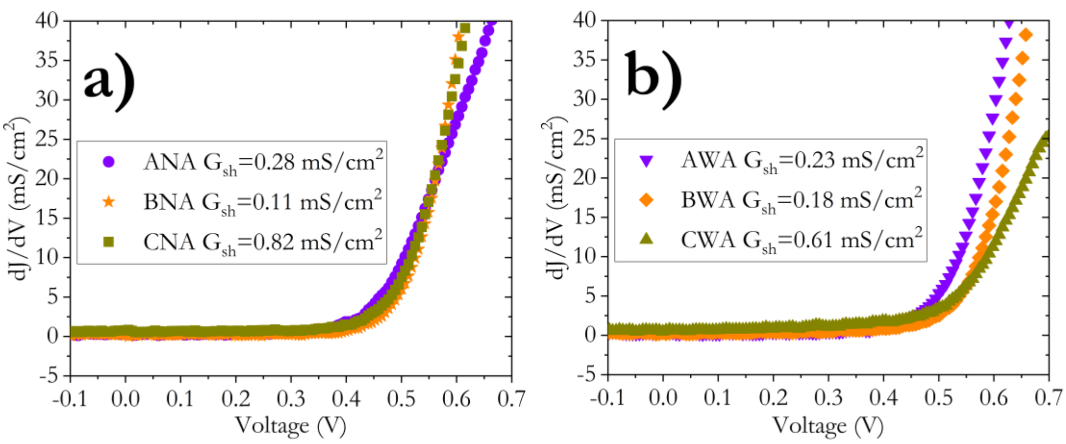

Fig. S7. Conductance (G_{sh}) of the samples a) without Al_2O_3 and b) with Al_2O_3.

In Fig. S8 are shown the curves to obtain series resistance (R_s) and ideality factor (A) values. Fig. S8a) showed the less R_s in sample BNA (6.0 Ωcm^2) and it showed an ideality factor of 1.7. On the other hand, sample BWA showed a Rs of 6.8 Ωcm^2 and an ideality factor of 1.8. Samples ANA and CWA showed the highest Rs values (12.4 Ωcm^2 and 19.7 Ωcm^2, respectively).

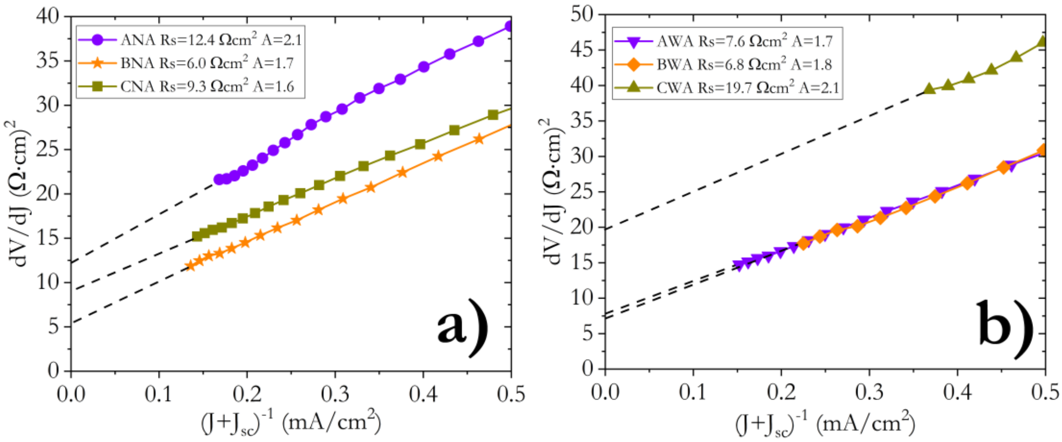

Fig. S8. Series resistance (Rs) and ideality factor (A) of the samples a) without Al_2O_3 and b) with Al_2O_3.

In Fig. S9 are shown the curves to obtain saturation current density (J_0) values. Fig. S9a) showed in sample BNA a saturation current density of 2.8x10^{-3} mA/cm^2 and in Fig. S9b) a saturation current density of 2.6x10^{-3} mA/cm^2. These values showed a major probability of recombination in these samples, but a decrease in J_0 from BWA showed a possible passivation in CZTS/CdS interface due to Al_2O_3. In samples ANA and CNA showed J_0 values of 1.6x10^{-5} mA/cm^2 and 5.5x10^{-7} mA/cm^2, respectively. In samples AWA and CWA showed J_0 values of 2.8x10^{-5} mA/cm^2 and 1.6x10^{-3} mA/cm^2.

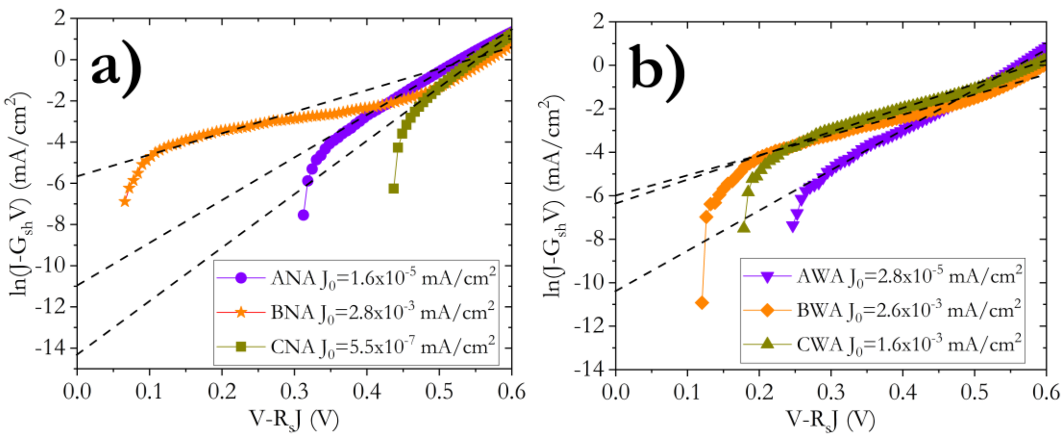

Fig. S9. Reverse saturation current density (J_0) of the samples a) without Al_2O_3 and b) with Al_2O_3.

In Table SII are shown the electrical parameter from CZTS solar cells on FTO substrate without and with Al_2O_3 passivation layer. Sample BWA showed 700 mV which is the best V_{oc} value, a current density of 18.2 mA/cm^2 and an efficiency of 7.3%. This means that Al_2O_3 helps to increase the V_{oc}, comparing with BNA which showed 677 mV in Voc. The V_{oc} of all the samples is in the range of 609-700 mV. The bandgap (E_g) of the samples are quite similar showing E_g in the range of 1.47-1.51 eV. Finally, sample BWA showed a $V_{oc(SQ)}$ deficit of 523 mV which is close to the best values reported in sulfur kesterite solar cells on molybdenum substrate (501 mV [S9], 503 mV [S10], 495 mV [S10]).

Table SII. Electrical parameters from the CZTS solar cells over FTO, without and with Al_2O_3. The values for the best solar cell from samples BNA and BWA are shown in brackets.

Sample	J_{sc} (mA/cm^2)	V_{oc} (mV)	FF (%)	η (%)	R_s (Ω·cm^2)	G_{sh} (mS/cm^2)	R_{sh} (Ω·cm^2)	A	J_0 (mA/cm^2)	$V_{oc(SQ)}$ deficit (mV)	Eg (eV)
ANA	14.9	609	53.6	4.9	12.4	0.28	3751.5	2.1	1.6×10^{-5}	659	1.51
BNA	17.2(17.8)	659(677)	61.1(63.8)	6.9 (7.7)	6.0	0.11	9091.0	1.7	2.8×10^{-3}	579(561)	1.50
CAN	13.7	628	56.4	4.9	9.3	0.82	1219.6	1.6	5.5×10^{-7}	620	1.47
AWA	15.5	648	55.3	5.5	7.6	0.23	4347.9	1.7	2.8×10^{-5}	605	1.51
BWA	17.7(18.2)	699(700)	56(57)	6.8 (7.3)	6.8	0.18	5555.6	1.8	2.6×10^{-3}	524(523)	1.50
CWA	13.6	645	50.7	4.4	19.7	0.61	1639.4	2.1	1.6×10^{-3}	621	1.47

In Fig. S10 are showed a) EQE response and b) integrated J_{sc} from samples BNA and BWA. Analyzing both sample BNA and BWA there is no difference between the J_{sc} measured and J_{sc} integrated (both showed difference of ~0.75 mA/cm^2).

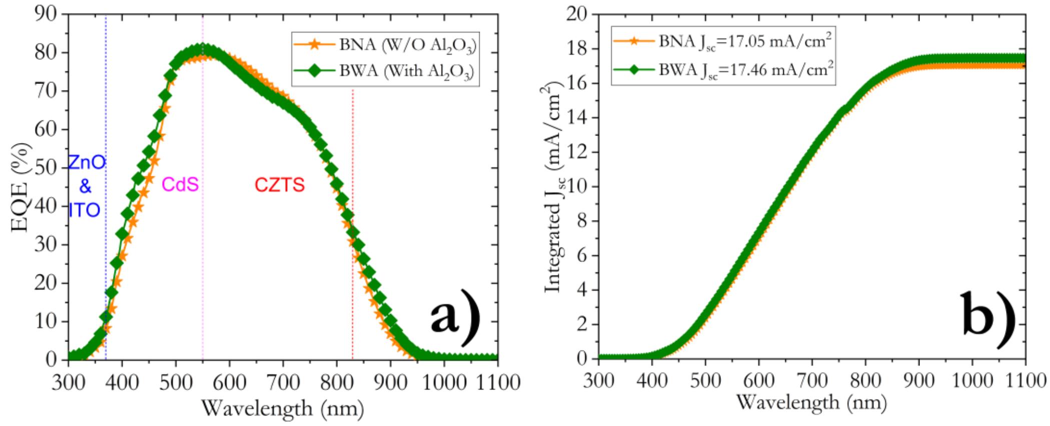

Fig. S10. a) EQE & b) Jsc integrated from CZTS solar cells (BNA and BWA) onto FTO substrate.

On the other hand, the external quantum efficiencies (EQE) are shown in Fig. S11. The sample AWA showed very good response in all the CZTS region (550-850 nm). In samples BNA and BWA, the response of both samples is very good, reaching 80% in response. In the same way, there is a better response for the sample BWA on the 500-600 nm region but, not a good response in the CZTS region (550-850 nm). Finally, samples CNA and CWA showed an EQE of 65%, approximately. The response of CNA is slightly better than CWA in CZTS region.

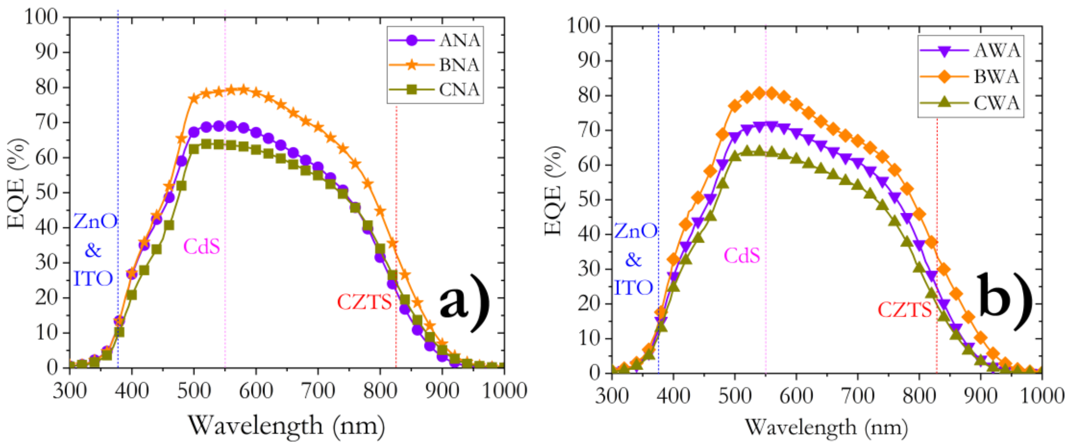

Fig. S11. EQE of CZTS solar cells onto FTO substrate of samples a) without Al_2O_3 and b) with Al_2O_3.

Additional Reference.

[S1] M. Guc, S. Levcenko, I. V. Bodnar, V. Izquierdo-Roca, X. Fontane, L. V. Volkova, E. Arushanov, A. Pérez-Rodríguez. "Polarized Raman scattering study of kesterite type Cu2ZnSnS4 single crystals". Sci. Rep. Vol. 6, 19414, 2016. DOI:10.1038/srep19414.

[S2] W. Li, J. Chen, C. Yan, X. Hao. "The effect of ZnS segregation on Zn-rich CZTS thin film solar cells". J. Alloy. Compd. 632 (2015) 178-184. DOI: 10.1016/j.jallcom.2015.01.205.

[S3] O. Awadallah, Z. Cheng. "In Situ Raman characterization of Cu2ZnSnS4 solar absorber material". 2015 IEEE 42nd Photovoltaic Specialist Conference (PVSC). DOI:10.1109/PVSC.2015.7355595.

[S4] J. Park, J. Huang, J. Yun, F. Liu, Z. Ouyang, H. Sun, C. Yan, K. Sun, K. Kim, J. Seidel, S. Chen, M.A. Green, X. Hao. "The role of hydrogen from ALD-Al2O3 in kesterite Cu2ZnSnS4 solar cells: grain surface passivation." Adv. Energy Mater. 1701940, 1-7, 2018. DOI: 10.1002/aenm.201701940.

[S5] M. E. Erkan, V. Chawla, M. A. Scarpulla. "Reduced defect density at the CZTSSe/CdS interface by atomic layer deposition of Al2O3". J. Appl. Phys. 2016, 119, 194504. DOI:10.1063/1.4948947.

[S6] G. Dingemans, W. M. M. Kessels. "Status and prospects of Al_2O_3-based surface passivation schemes for silicon solar cells". J. Vac. Sci. Technol. A, 30 040802 (2012). DOI: http://dx.doi.org/10.1116/1.4728205.

[S7] S. S. Hegedus, W. N. Shafarman. "Thin-film solar cells: device measurements and analysis". Prog. Photovolt: Res. Appl. 2004; 12: 155-176. DOI: 10.1002/pip.518.

[S8] I. Becerril-Romero, D. Sylla, M. Placidi, Y. Sánchez, J. Andrade-Arvizu, V. Izquierdo-Roca, M. Guc, A. Pérez-Rodríguez, S. Grini, L. Vines, B. Pusay, R. Almache, J. Puigdollers, P. Pistor, E. Saucedo and M. Espíndola-Rodríguez. "Transition-Metal Oxides for Kesterite Solar Cells Developed on Transparent Substrates". ACS Appl. Mater. Interfaces 2020, 12, 30, 33656-33669. DOI:10.1021/acsami.0c06992.

[S9] C. Yan J. Huang, K. Sun, S. Johnston, Y. Zhang, H. Sun, A. Pu, M. He, F. Liu, K. Eder, L. Yang, J.M. Cairney, N.J. Ekins-Daukes, Z. Hameiri, J.A. Stride, S. Chen, M.A. Green, X. Hao. "Cu2ZnSnS4 solar cells with over 10% power conversion efficiency enabled by heterojunction heat treatment". Nature energy. 3, 764-772 (2018). DOI: 10.1038/s41560-018-0206-0.

[S10] S. Bourdais, C. Choné, B. Delatouche, A. Jacob, G. Larramona, C. Moisan, A. Lafond, F. Donatini, G. Rey, S. Siebentritt, A. Walsh, G. Dennler. "Is the Cu/Zn disorder the main culprit for the voltage deficit in kesterite solar cells?" Adv. Energy Mater. 2016, 6, 1502276. DOI: 10.1002/aenm.201502276.